Available online at www.sciencedirect.com
SCIENCE DIRECT®
Journal of Sound and Vibration 273 (2004) 219–231
JOURNAL OF SOUND AND VIBRATION
www.elsevier.com/locate/jsvi

# Free in-plane vibration of isotropic non-rectangular plates

A.V. Singh*, T. Muhammad

*Department of Mechanical and Materials Engineering, Faculty of Engineering, The University of Western Ontario, London, Ont., Canada N6A 5B9*

Received 20 November 2002; accepted 15 April 2003

**Abstract**

A numerical study for the free in-plane vibration of non-rectangular plate is presented in this paper. The plate is defined by four curved boundaries using eight points and natural co-ordinates to map the geometry. The displacement nodes are introduced at the boundary of the plate as well as inside the perimeter. Each displacement node has two degrees of freedom and much higher order polynomials than the ones used for the geometric representation are used to represent the displacement fields. Using the energy functional, the matrix equation is obtained and solved for natural frequencies and associated mode shapes. Numerical results are calculated first for rectangular plates with three sets of boundary conditions and then compared with the data published in the literature by other researchers. Additional results are also presented and discussed in this paper for the in-plane vibration of rhombic and circular–annular–sector plates.


## 1. Introduction

The flexural vibration of plates has been studied with considerable interest for nearly 100 years and the results are available for a wide range of shapes and boundary conditions [1]. Generally, the flexural modes occur at low frequencies. However, vibrating plates also have in-plane modes at relatively high frequencies and can be of very practical significance in aerospace structures, which operate at very high speeds.

Chen and Liu [2] studied in-plane vibration of elliptical, triangular, square and hexagonal plates by considering plane stress criterion in the governing differential equation. The boundary conditions were satisfied by the least square method. A method was presented by Nagaya [3] for the free vibration analysis of an arbitrarily shaped membrane with point supports. In this paper, an elliptical plate with two point supports symmetrically located on the major axis was considered as the

*Corresponding author. Tel.: +1-519-661-2111; fax: +1-519-661-3020.
*E-mail address:* avsingh@eng.uwo.ca (A.V. Singh).

0022-460X/03/$ - see front matter 
doi:10.1016/S0022-460X(03)00496-6

numerical example. Dimensionless natural frequencies of the free in-plane axially symmetric and asymmetric vibrations of thin annular plates with free–free, free–clamped, clamped free and clamped–clamped boundary conditions, are found in the work by Irie et al. [4]. The numerical calculations have been carried out by using the transfer matrix method which, according to them, is simple and assures an accuracy sufficient for practical purposes. Irie and co-investigators [5] also studied a point-supported rectangular membrane, symmetrical with respect to the center lines and stretched by inextensible strings. Kobayashi et al. [6] studied the frequencies and mode shapes of in-plane vibration of rectangular plates supported at four points symmetrically located with respect to the two principal axes. Also referenced in this paper are two papers published in Japanese on the in-plane vibrations of rectangular plates by the finite element method.

Bardell et al. [7] considered simply supported, clamped and free rectangular plates and studied the in-plane vibration using the Rayleigh–Ritz method. In their paper, values of the natural frequencies along with the mode shapes are presented for square as well as rectangular plates having the aspect ratio of 2. The paper by Bercin and Langley [8] dealt with the application of the dynamic stiffness technique to the in-plane vibrations of plate structures, namely a ship foundation and hull. Farag and Pan [9] developed a mathematical model for predicting the forced response of a rectangular plate clamped on all sides to the in-plane point force excitations and compared the predicted resonant frequencies and mode shapes against the results obtained using NASTRAN. Using the Kantorovich–Krylov variational method, Wang and Wereley [10] analytically solved for the modal frequencies and mode shapes of the in-plane vibration of rectangular plates with combinations of free and clamped boundary conditions. They validated the first six natural frequencies using NASTRAN for which the model consisted of 480 four nodded elements.

It appears that in-plane vibrations of rectangular and circular annular plates received attention from researchers and a good amount of numerical results is available in the literature. But the in-plane vibration of non-rectangular plates, which is the focus of the present study, has received very limited to no attention of the researchers. In the present study, the plate geometry is defined by a region bounded by four curved edges, with end points and the mid-point co-ordinates of each edge being prescribed, and then mapped using the natural co-ordinates. The displacement fields are deduced using relatively higher order polynomials than the ones used for defining region within the plate boundary. A grid of $(p+1)\times(q+1)$ points, where $p$ and $q$ are the orders of the polynomials in the two natural co-ordinates, is introduced as the displacement nodes. Each of the displacement nodes is assigned two degrees of freedom along the $x$ and $y$ axes respectively. The matrix equation of motion is derived from the variational approach, i.e., the stationarity of the potential energy functional. Numerical method is validated first by comparing results from the present investigation for rectangular and square plates with the published data of Bardell et al. [7] and Wang and Wereley [10]. Some additional results pertaining to frequencies and mode shapes of rhombic and circular annular sector plates are also presented and discussed in this paper. It is believed that the present method is very effective and yields accurate results with significantly fewer degrees of freedom than the finite element method.

## 2. Definition of the geometry

The quadrilateral region of the plate being studied for the in-plane vibration is bounded by a set of four curved edges in the $x$-$y$ plane as shown in Fig. 1. This region is considered to represent the

middle surface of the plate of which the thickness ($h$) is assumed to be uniform and small in comparison with the dimensions along $x$ and $y$ axes.

Co-ordinates of the four corner points are denoted by numerals 1–4 in a sequential counter clockwise sense. The middle edge points are numbered from 5 to 8 as shown in Fig. 1. The co-ordinates of the geometric nodes at the middle plane are expressed by $x(j)$, $y(j)$ with $j=1, 2, 3, \ldots,8$ and are known. In this study the natural co-ordinates $\xi$ and $\eta$, bounded by $-1\leqslant(\xi \text{ or } \eta)\leqslant+1$, together with the shape functions $N_j$ $(\xi, \eta)$ for $j=1,2,3,\ldots,8$ are used to interpolate the co-ordinates $(x, y)$ of an arbitrary point inside the quadrilateral region [11].

$$x(\xi,\eta)=\sum_{j=1}^{8} N_j(\xi,\eta)\, x_j, \quad y(\xi,\eta)=\sum_{j=1}^{8} N_j(\xi,\eta)\, y_j. \tag{1}$$

From here on, all the functional forms of the plate quantities are expressed in terms of the parametric co-ordinates $\xi$ and $\eta$. The Jacobian matrix $[J(\xi,\eta)]$ and its determinant $|J(\xi,\eta)|$ are used in the derivation of the plate equations which follow.

Assume that the plate under consideration undergoes the in-plane motion only and $u$ and $v$ denote respectively the displacement components in $x$ and $y$ directions. The strain–displacement relations under this condition are given by

$$\varepsilon_x=\frac{\partial u}{\partial x}, \quad \varepsilon_y=\frac{\partial v}{\partial y}, \quad \gamma_{xy}=\frac{\partial u}{\partial y}+\frac{\partial v}{\partial x}. \tag{2}$$

Also, the stress strain relation is $\{\sigma\}=[E]\{\varepsilon\}$, where $\{\sigma\}^{\mathrm{T}}=\{\sigma_x\ \sigma_y\ \tau_{xy}\}$; $\{\varepsilon\}^{\mathrm{T}}=\{\varepsilon_x\ \varepsilon_y\ \gamma_{xy}\}$ and

$$[E]=\frac{E}{1-v^2}\begin{bmatrix} 1 & v & 0 \\ v & 1 & 0 \\ 0 & 0 & \dfrac{1-v}{2} \end{bmatrix} \tag{3}$$

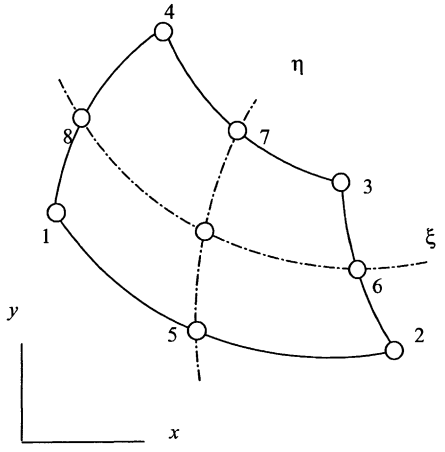


Fig. 1. Geometry of the plate.

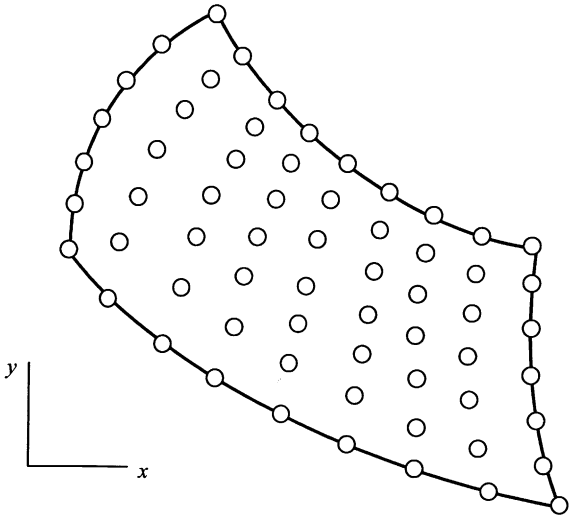


Fig. 2. The displacement nodes for the plate segment.

The potential energy function for the in-plane vibration of the plate is

$$\Pi = (1/2)\, h \int_{-1}^{+1} \int_{-1}^{+1} \left[\{\varepsilon\}^{\mathrm{T}}([E])\{\varepsilon\} - \omega^2(u^2 + v^2)\right] |J(\xi,\eta)|\ \mathrm{d}\xi\ \mathrm{d}\eta. \tag{4}$$

So far we have discussed the natural co-ordinates in conjunction with the quadrilateral geometric shape and the elasticity equations. Now, we proceed to develop the equation of motion governing the in-plane vibration of the plate. The generic displacement components $u$ and $v$ are described by the following polynomials:

$$u = \sum_{j=1}^{n} u_j \psi_j(\xi,\eta), \quad v = \sum_{j=1}^{n} v_j \psi_j(\xi,\eta). \tag{5}$$

Application of the above equation can be made using a grid of displacement nodes similar to the $9 \times 7$ grid of 63 points shown in Fig. 2. This grid of displacement nodes corresponds to the eighth and sixth order polynomials in $\xi$ and $\eta$ respectively. Each grid point is assigned two degrees of freedom, e.g., the jth grid point has two degrees of freedom $u_j$ and $v_j$ respectively. The interpolation polynomials $\psi_j(\xi,\eta)$ for $j=1$ to $n$ in Eq. (5) can be deduced in the same manner as $N_j(\xi,\eta)$ in Eq. (1). In the present formulation, eight nodal points are used for the geometry definition, whereas $n = (p+1)(q+1)$ displacement nodes are used. Indices $p$ and $q$ denote respectively the orders of the polynomials in $\xi$ and $\eta$. Eq. (5) is written in the following matrix form:

$$\{\Delta\} = \left[[\psi_1(\xi,\eta)]\ [\psi_2(\xi,\eta)]\ [\psi_3(\xi,\eta)]\ [-]\ [-]\ [\psi_n(\xi,\eta)]\right]\{Q\}, \tag{6}$$

where $\{\Delta\}^{\mathrm{T}} = \{u\ \ v\}, \{Q\}^{\mathrm{T}} = \{u_1\ \ v_1\ \ u_2\ \ v_2\ \ u_3\ \ v_3\ \ u_4\ \ v_4 .. \ ..\text{etc.}\}$ and contains displacements at each displacement node. Matrix $[\psi_j(\xi,\eta)]_{2\times 2}$ for the $j$th displacement node is given by

$$[\psi_j(\xi,\eta)] = \begin{bmatrix} \psi_j(\xi,\eta) & 0 \\ 0 & \psi_j(\xi,\eta) \end{bmatrix}. \tag{7}$$

By substituting Eq. (5) into Eq. (2), we get

$$\{\varepsilon\} = [B]\ \{Q\}. \tag{8}$$

Substituting Eq. (8) into Eq. (4), we obtain the stiffness matrix for the linear part,

$$\Pi = (1/2)\ \{Q\}^{\mathrm{T}}(h[k] - \rho h\omega^2[m])\{Q\}, \tag{9}$$

where $[k] = \int_{-1}^{+1}\int_{-1}^{+1}[B]^{\mathrm{T}}[E]\,[B]\,|J(\xi,\eta)|\,\mathrm{d}\xi\,\mathrm{d}\eta$ and $[m] = \int_{-1}^{+1}\int_{-1}^{+1}[A]^{\mathrm{T}}\,[A]\,|J(\xi,\eta)|\,\mathrm{d}\xi\,\mathrm{d}\eta$.

We have derived the stiffness and mass matrices for the plate. Integration here can be carried over numerically, e.g., Gaussian quadrature for which the number of integration points selected will depend upon the order of the polynomial used in defining the displacement fields. From the stationarity of the potential energy function, we obtain the following eigenvalue/eigenvector matrix equation:

$$([k] - \Omega^2[m])\{q\} = 0, \quad \text{where} \quad \Omega = \omega a\sqrt{\rho/E}. \tag{10}$$

## 3. Numerical results and discussions

The present numerical method is a modified form of the Rayleigh–Ritz method in which the shape functions are used as the admissible displacement fields. These shape functions are generated using complete polynomials in both natural co-ordinates $\xi$ and $\eta$. The use of complete functions provides a continuous representation of the displacement fields throughout the domain as well as enhances the computational stability. The boundary conditions are enforced on the displacement nodes. If a particular displacement condition applies to the entire edge, that condition ought to be applied to all the nodes falling on this edge. Also, this approach permits the analysis of plates with partial constraints along an edge, or the plate supported at only a few discrete points. For convergence and better accuracy, geometry is kept unchanged and the analysis is repeated by increasing the orders of the interpolating functions. In finite element analysis, both the geometry and the displacement fields are refined. Displacement continuity in finite element method is enforced only on the nodal points. But the displacement field in the present method is continuous over the entire region of the plate. Any approximation associated with an element accumulates as the number of elements is increased in the analysis. This is not the case in the present formulation. By mapping of the domain in this investigation, it is possible to analyze different types of plates, which are considered in the following as numerical examples.

Two geometric shapes of the plate are considered in the present numerical investigation. The first is a parallelogram plate defined by the lengths of the sides ($a$ and $b$) and the angle $\alpha$ as shown in Fig. 3. Similarly, Fig. 4 shows the second plate type, which is an annular circular sector plate defined by the outside radius ($a$), inside radius ($b$) and subtending angle ($\alpha$). Typically, the geometry is defined by eight points as shown in these figures for the respective cases. With regards to the displacement nodal points, the model is based on eighth order polynomial in each of $\xi$ and $\eta$ directions. This order of polynomial creates a model with the grid of $9 \times 9$ nodal points, each having two degrees of freedom corresponding to $u$ and $v$. In all, there are 162 degrees of freedom in the model, and eigenquation involving the 162nd order matrix is solved for the natural frequencies and associated mode shapes. For numerical integration, nine Gauss points are used in

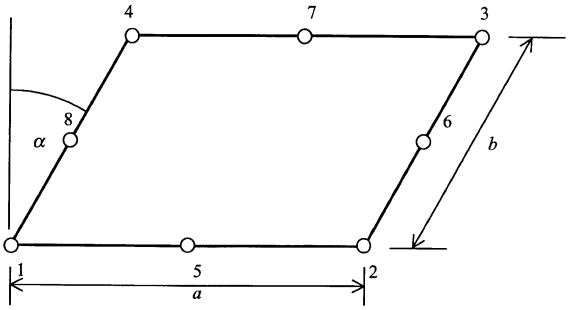


Fig. 3. Parallelogram plate.

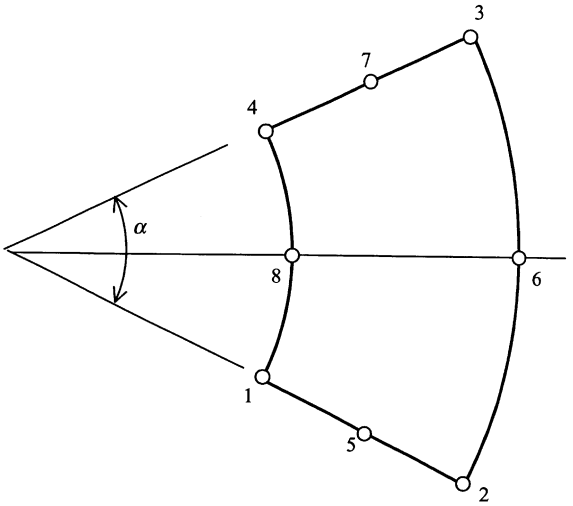


Fig. 4. Circular annular sector plate.

each of $\xi$ and $\eta$ directions. In order to determine the effectiveness and validity of the present method, square and rectangular plates are analyzed first and numerical results are compared with those of others from the literature. For the analysis of rectangular plates, the geometry shown in Fig. 3 is used with angle $\alpha = 0$.

### 3.1. Rectangular and square plates

Bardell et al. [7] presented values of the natural frequencies and corresponding mode shapes for square and rectangular (having aspect ratio of 2) plates using Rayleigh–Ritz method for the analysis (Table 1). Square plate with all sides clamped is analyzed by the present method and results up to six modes are compared with the same from the above mentioned work as shown below:

| | | | | | |
|---|---|---|---|---|---|
| 3.727 | 3.727 | 4.400 | 5.436 | 6.1605 | 6.174 |
| (3.727) | (3.727) | (4.400) | (5.436) | (6.142) | (6.180). |

Table 1
Natural frequencies in hertz for the in-plane vibration of rectangular plate

| Mode no. | Present | Wang and Wereley [10] | | Farag and Pan [9] |
|---|---|---|---|---|
| | | NASTRAN | Analytical | |
| | | *CCCC boundary conditions* | | |
| 1 | 2665.42 | 2658 | 2667 | 2671 |
| 2 | 2905.32 | 2898 | 2909 | 2914 |
| 3 | 3277.78 | 3260 | 3280 | 3349 |
| 4 | 4050.31 | 4024 | 4089 | 4198 |
| 5 | 4307.11 | 4268 | 4327 | 4404 |
| 6 | 4429.43 | 4404 | 4437 | 4607 |
| | | *CCCF boundary conditions* | | |
| 1 | 1804.62 | 1803 | 1811 | 1892 |
| 2 | 2660.02 | 2656 | 2674 | 2727 |
| 3 | 2802.48 | 2794 | 2845 | 3026 |
| 4 | 3406.56 | 3392 | 3524 | 3596 |
| 5 | 3492.26 | 3479 | 3504 | 3624 |
| 6 | 3729.41 | 3704 | 3757 | 3868 |
| | | *CFCF boundary conditions* | | |
| 1 | 1448.25 | 1449 | 1455 | 1531 |
| 2 | 2516.37 | 2511 | 2520 | 2682 |
| 3 | 2569.37 | 2567 | 2639 | 2697 |
| 4 | 2642.75 | 2637 | 2662 | 2994 |
| 5 | 3037.66 | 3037 | 3187 | 3122 |
| 6 | 3069.49 | 3061 | 3146 | 3390 |

Plate dimensions: 1000 mm × 1200 mm × 2.5 mm. Material properties: $E = 70 \times 10^9$ N/m$^2$, $v = 0.33$, $\rho = 2700$ kg/m$^3$.

The results from Bardell et al. [7] are given in parentheses. The associated mode shapes also exhibited behaviour same as that found in this reference.

Another comparison of results from the present study is made with those of Farag and Pan [9] and Wang and Wereley [10]. In these two papers, values of the natural frequencies in hertz are presented for the plate with dimensions 1.0 m × 1.2 m × 2.5 mm and material properties: Young's modulus $E = 70$ GPa, mass density $\rho = 2700$ kg/m$^3$ and Poisson's ratio $v = 0.33$. They considered three sets of boundary conditions, namely, CCCC (i.e., all sides fixed), CCCF (i.e., three sides fixed and the fourth one free) and CFCF (a case combining fixed and free conditions). Parameters used for this comparison are $b/a = 1.2$ and $\alpha = 0$. For fixed edge both $u$ and $v$ are set to zero. For CCCF case, boundaries represented by edges 1–4, 1–2 and 2–3 are considered to be fixed and 3−4 is assumed to be free. Similarly, for CFCF case, boundaries represented by edges 1−4 and 2−3 are fixed and edges 1−2 and 3−4 are set free. The results from the present investigation are consistently lower than those obtained analytically by Farag and Pan [9] and Wang and Wereley [10]. However, the NASTRAN results are lower than the present ones, which match much better with the NASTRAN

results than those from earlier investigations by other researchers. The maximum percentage difference between the present set of results and those from NSTRAN is less than one per cent.

### 3.2. Rhombic plates

The rhombic plate is analyzed for the same three combinations of boundary conditions as the rectangular plate discussed above. Though one can use the symmetry conditions about the diagonals of the rhombus and carry out the analysis using only one-quarter of the plate, the full plate with 81 displacement grid points is considered in the present calculation. Table 2 presents frequencies $\Omega = \omega a\sqrt{\rho/E}$ for the first six modes of vibration. By considering $\alpha$ from $0^\circ$ to $60^\circ$, this table contains the values of the natural frequencies of square plate to highly acute rhombus. It is noted from the table that frequency increases as angle increases for all cases. Also, the values of the frequencies increase as the number of fixed edges increases. The first six mode shapes for a $45^\circ$ rhombus with all clamped boundaries are plotted and shown in Fig. 5. When the simulation was done on these mode shapes, the following observations were noted. In the first mode corresponding to $\Omega = 4.3404$, oscillatory motion occurred about the short diagonal represented

Table 2
Frequency $\Omega = \omega a\sqrt{\rho/E}$ for the in-plane vibrating rhombic plate with the Poisson ratio $v = 0.33$

| Mode no. | $\alpha = 0.0$ | $\alpha = 15.0$ | $\alpha = 30.0$ | $\alpha = 45.0$ | $\alpha = 60.0$ |
|---|---|---|---|---|---|
| | | *CCCC boundary conditions* | | | |
| 1 | 3.7270 | 3.6814 | 3.8498 | 4.3407 | 5.5372 |
| 2 | 3.7270 | 3.9743 | 4.4861 | 5.4588 | 7.5428 |
| 3 | 4.4395 | 4.5708 | 5.0125 | 5.9608 | 7.5231 |
| 4 | 5.4363 | 5.4862 | 5.6953 | 6.2334 | 8.0737 |
| 5 | 6.1601 | 6.1674 | 6.5262 | 7.4494 | 9.3394 |
| 6 | 6.1741 | 6.2888 | 6.7847 | 7.9611 | 9.7038 |
| | | *CCCF boundary conditions* | | | |
| 1 | 2.3801 | 2.4390 | 2.6360 | 3.0521 | 3.9428 |
| 2 | 3.3165 | 3.3865 | 3.6174 | 4.1027 | 5.1716 |
| 3 | 3.5742 | 3.6678 | 3.9792 | 4.6204 | 5.9077 |
| 4 | 4.5148 | 4.5572 | 4.7449 | 5.2293 | 6.4405 |
| 5 | 4.9459 | 5.0827 | 5.1358 | 6.1184 | 7.6716 |
| 6 | 5.1970 | 5.2633 | 5.6158 | 6.4821 | 7.9042 |
| | | *CFCF boundary conditions* | | | |
| 1 | 1.7758 | 1.8283 | 2.0040 | 2.3776 | 3.1955 |
| 2 | 3.1653 | 3.2360 | 3.4737 | 3.7975 | 4.9137 |
| 3 | 3.2713 | 3.3225 | 3.5010 | 3.9587 | 5.0550 |
| 4 | 3.5130 | 3.6059 | 3.8486 | 4.2501 | 5.1719 |
| 5 | 3.9266 | 4.0097 | 4.3282 | 4.8358 | 5.9619 |
| 6 | 4.0912 | 4.1498 | 4.3569 | 5.0693 | 6.5640 |

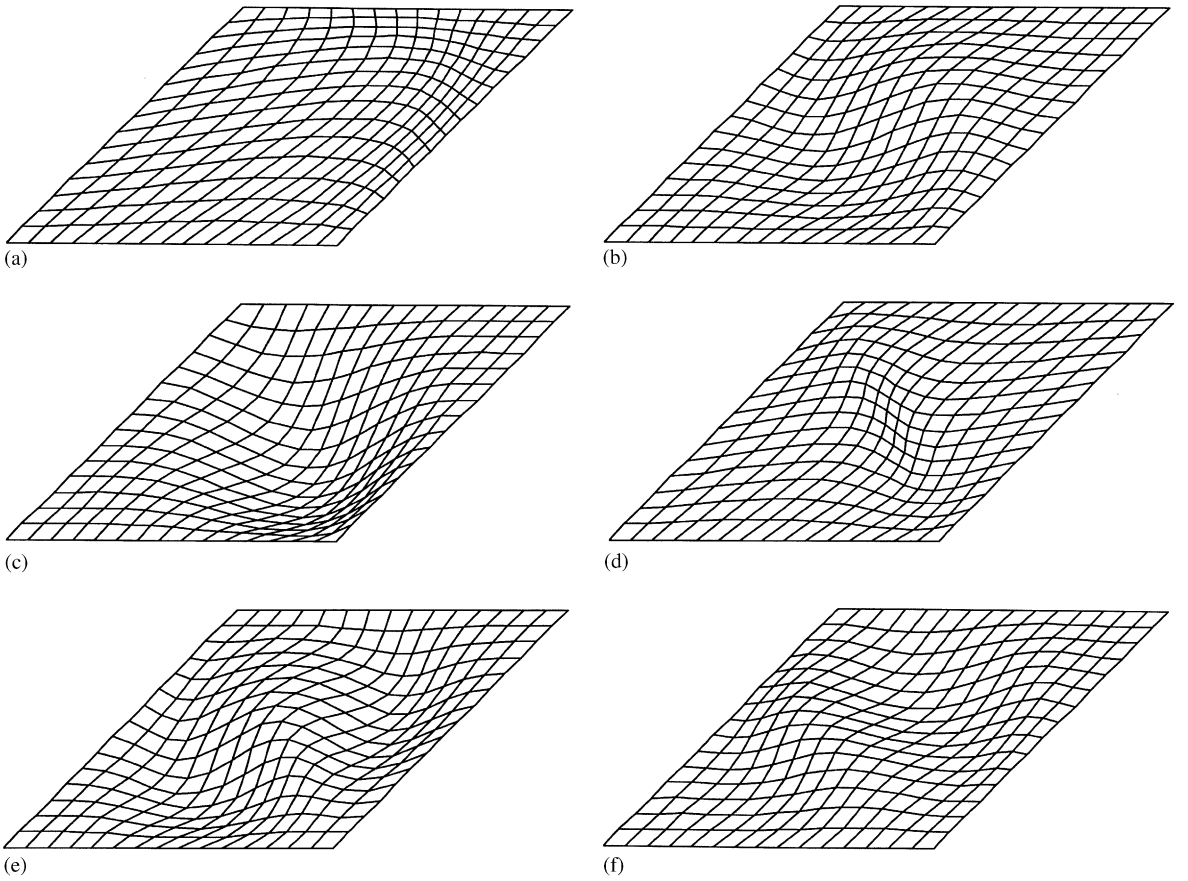


Fig. 5. Mode shapes for a 45° rhombic CCCC plate: (a) mode # 1 ($\Omega = 4.3404$), (b) mode # 2 ($\Omega = 5.4588$), (c) mode # 3 ($\Omega = 5.9608$), (d) mode # 4 ($\Omega = 6.2334$), (e) mode # 5 ($\Omega = 7.4494$), (f) mode # 6 ($\Omega = 7.9611$).

by 2–4 in Fig. 3. The entire plate appeared to move in the direction perpendicular to it. Similarly, for the case of the second mode corresponding to $\Omega = 5.4588$, the motion took place in the direction perpendicular to the long diagonal represented by 1–3. Also, the motion occurred perpendicular to the long diagonal in the third mode for which to $\Omega = 5.9608$. But one half moved down while the other half up the diagonal and the mode can be characterized by the in-plane shear mode. The two halves of the plate about the short diagonal move in the direction of the long diagonal in mode 4 with $\Omega = 6.2334$. They show simultaneously movements either away or towards the small diagonal on which points oscillate along it, not out of it. Mode 5 is an in-plane shear mode similar to mode 3 with the difference that the three segments of the plate show oscillation perpendicular to the long diagonal, if segment about the short diagonal moves up, the other two segments which are mirror image of each other about the short diagonal move down. Mode 6 is also of the shear type with two segments, of the plate on each half about the short diagonal, moving in oppositions. The motion characteristics are shown in Fig. 6.

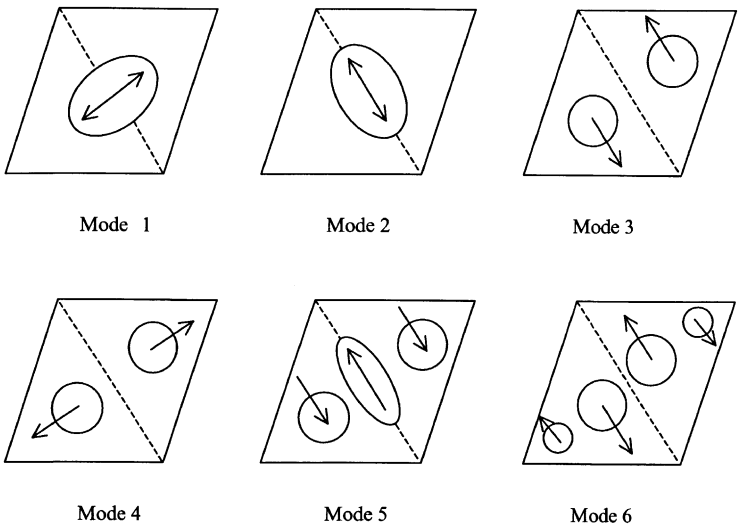


Fig. 6. Vibratory characteristics of a CCCC 45° rhombic plate.

Table 3
Frequency $\Omega = \omega a\sqrt{\rho/E}$ for the in-plane vibrating annular sector plate with the Poisson ratio $v = 0.3$ and ratio of inside to outside radii $b/a = 0.5$.

| Mode no. | $\alpha = 30.0$ | $\alpha = 45.0$ | $\alpha = 60.0$ | $\alpha = 75.0$ | $\alpha = 90.0$ |
|---|---|---|---|---|---|
| | | *CCCC boundary conditions* | | | |
| 1 | 8.1592 | 6.6113 | 5.5963 | 5.0629 | 4.7576 |
| 2 | 8.8379 | 7.2730 | 6.9235 | 6.7002 | 6.3458 |
| 3 | 10.1089 | 8.1863 | 7.4305 | 7.0684 | 6.9512 |
| 4 | 12.7648 | 10.3517 | 8.6325 | 7.4864 | 6.9793 |
| 5 | 13.2623 | 10.6104 | 9.0380 | 8.0930 | 7.5749 |
| 6 | 13.2555 | 10.8649 | 9.2545 | 8.6133 | 8.0831 |
| | | *CCCF boundary conditions* | | | |
| 1 | 5.3158 | 4.4936 | 4.1930 | 4.0631 | 4.0055 |
| 2 | 6.8500 | 6.5548 | 6.3518 | 5.9032 | 5.4345 |
| 3 | 7.4560 | 6.9123 | 6.7162 | 6.6534 | 6.5046 |
| 4 | 10.2296 | 8.5881 | 7.1459 | 6.6604 | 6.6321 |
| 5 | 10.7897 | 8.5840 | 7.8030 | 7.3121 | 7.0237 |
| 6 | 11.5210 | 9.3230 | 8.1970 | 7.7075 | 7.3563 |
| | | *CFCF boundary conditions* | | | |
| 1 | 3.4489 | 3.6116 | 3.6912 | 3.7422 | 3.7834 |
| 2 | 6.2700 | 5.8880 | 5.1823 | 4.7354 | 4.4797 |
| 3 | 6.4037 | 6.4635 | 6.4017 | 6.3011 | 6.0711 |
| 4 | 8.3676 | 6.6862 | 6.4919 | 6.5000 | 6.5393 |
| 5 | 8.3358 | 7.5640 | 7.0363 | 6.7543 | 6.5952 |
| 6 | 9.4104 | 7.6711 | 7.2645 | 7.0761 | 6.7786 |

### 3.3. Circular annular sector plate

In this case a circular annular plate as shown in Fig. 4 is considered. The outside and inside radii for this problem are denoted by $a$ and $b$ respectively and the subtended angle by $\alpha$. Edges 1–8–4, 1–5–2, 2–6–3 and 3–7–4 are designated by 1 through 4. For numerical results subtending angles 30°, 45°, 60°, 75° and 90° have been considered along with $b/a = 0.5$. Presented in Table 3 are the values of the first six modes of circular sector plates for three sets of boundary conditions CCCC, CCCF and CFCF. For the first two cases, i.e., CCCC and CCCF, values of natural frequency decrease as angle $\alpha$ increases. For the case with CFCF, the natural frequency for the

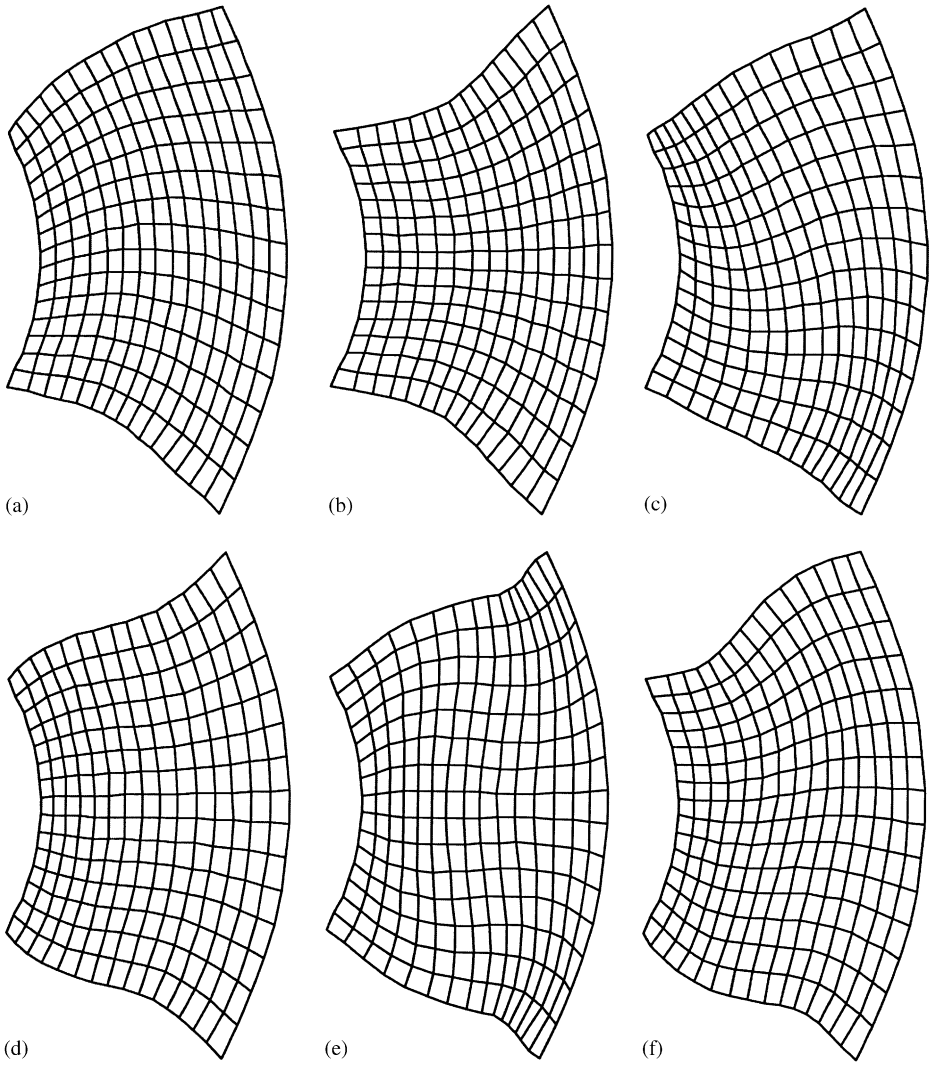


Fig. 7. Mode shapes for a 60° annular sector CFCF plate: (a) mode # 1($\Omega = 3.6912$), (b) mode # 2 ($\Omega = 5.1823$), (c) mode # 3 ($\Omega = 6.4017$), (d) mode # 4 ($\Omega = 6.4919$), (e) mode # 5 ($\Omega = 7.0363$), (f) mode # 6 ($\Omega = 7.2645$).

fundamental modes of sector plates increases with angle $\alpha$. However, the frequencies associated with higher modes also do not show the same behaviour as the other two combinations of boundary conditions. Mode shapes for the CFCF case are also presented in Fig. 7 in which two types of vibrating modes are seen. In modes 1, 3 and 6 the entire plate oscillates in its plane in the circumferential direction with higher radial wave numbers. In modes 2, 4 and 5, the vibrating modes appear to be symmetrical about the radial line 8–6. The plate motion in these symmetric vibrating modes can be described by saying that both halves of the plates either move together either inward or outward with reference to the line of symmetry.

## 4. Concluding remarks

A numerical investigation of the in-plane vibration of non-rectangular plate has been presented in this paper. The plate geometry is defined by four curved edges with eight nodal points and mapped into a square using natural co-ordinates $(\xi, \eta)$. For the displacement fields representing $u$ and $v$, considerably higher order polynomials, relative to those used for mapping the geometry, are used in the analysis. The displacement nodes are introduced on the boundary as well as inside it. The method is versatile and can be used for many types of plate geometry and boundary conditions, which can be enforced on the displacement nodes. In the finite element analysis, the accuracy of the results is improved by increasing the number of elements through mesh refinement. In the present method, the geometry is represented by one segment only, but the order of the polynomial is increased in the displacement fields for better accuracy in results. Though, by doing so, the number of displacement nodes is increased, and still more accurate results are obtained with a relatively smaller number of degrees of freedom than when using finite elements.

First numerical results are obtained by the present method for the free vibration of rectangular plates for which frequency data are available in the literature. Excellent agreement is found between the present results and those published by other researchers. Additional results are also presented and discussed in this paper for the in-plane vibration of rhombic and circular annular sector plates.

## References

[1] A.W. Leissa, Vibration of plates, NASA SP-160, US Government Printing Office, Washington, DC, 1969.
[2] S.S.H. Chen, T.M. Liu, Extensional vibration of thin plates of various shapes, *Journal of the Acoustical Society of America* 58 (4) (1975) 828–831.
[3] K. Nagaya, Vibration of an arbitrarily shaped membrane with point supports, *Journal of Sound and Vibration* 65 (1) (1979) 1–9.
[4] T. Irie, G. Yamada, Y. Muramoto, Natural frequencies of in-plane vibration of annular plates, *Journal of Sound and Vibration* 97 (1984) 171–175.
[5] T. Irie, G. Yamada, Y. Kobayashi, Free vibration of a point supported membrane stretched by inextensible strings, *Journal of Sound and Vibration* 93 (1984) 513–522.
[6] Y. Kobayashi, G. Yamada, S. Honma, In-plane vibration of point supported rectangular plates, *Journal of Sound and Vibration* 126 (3) (1988) 545–549.
[7] N.S. Bardell, R.S. Langley, J.M. Dunsdon, On the free in-plane vibration of isotropic rectangular plates, *Journal of Sound and Vibration* 191 (3) (1996) 459–467.

[8] A.N. Bercin, R.S. Langley, Application of the dynamic stiffness technique to the in-plane vibrations of plate structures, *Computers and Structures* 59 (5) (1996) 869–875.
[9] N.H. Farag, J. Pan, Free and forced in-plane vibration of rectangular plates, *Journal of the Acoustical Society of America* 103 (1) (1998) 408–413.
[10] G. Wang, N.M. Wereley, Free in-plane vibration of rectangular plates, *American Institute of Aeronautics and Astronautics, Journal* 40 (5) (2002) 953–959.
[11] W. Weaver, P.R. Johnston, *Finite Elements for Structural Analysis*, Prentice-Hall, Englewood Cliffs, NJ, 1984.